Optics Letters

Optically pumped 1.3 μm room-temperature InAs quantum-dot micro-disk lasers directly grown on (001) silicon

Yating Wan,[1,†] Qiang Li,[1,†] Alan Y. Liu,[2,†] Arthur C. Gossard,[2,3] John E. Bowers,[2,3] Evelyn L. Hu,[4] and Kei May Lau[1,*]

[1]Department of Electronic and Computer Engineering, Hong Kong University of Science and Technology, Clear Water Bay, Kowloon, Hong Kong, China
[2]Materials Department, University of California, Santa Barbara, California 93106, USA
[3]Department of Electrical and Computer Engineering, University of California, Santa Barbara, California 93106, USA
[4]School of Engineering and Applied Sciences, Harvard University, Cambridge, Massachusetts 02138, USA
*Corresponding author: eekmlau@ust.hk

Received 16 February 2016; revised 8 March 2016; accepted 9 March 2016; posted 10 March 2016 (Doc. ID 259455); published 1 April 2016

Direct integration of high-performance laser diodes on silicon will dramatically transform the world of photonics, expediting the progress toward low-cost and compact photonic integrated circuits (PICs) on the mainstream silicon platform. Here, we report, to the best of our knowledge, the first 1.3 μm room-temperature continuous-wave InAs quantum-dot micro-disk lasers epitaxially grown on industrial-compatible Si (001) substrates without offcut. The lasing threshold is as low as hundreds of microwatts, similar to the thresholds of identical lasers grown on a GaAs substrate. The heteroepitaxial structure employed here does not require the use of an absorptive germanium buffer and/or dislocation filter layers, both of which impede the efficient coupling of light from the laser active regions to silicon waveguides. This allows for full compatibility with the extensive silicon-on-insulator (SOI) technology. The large-area virtual GaAs (on Si) substrates can be directly adopted in various mature in-plane laser configurations, both optically and electrically. Thus, this demonstration represents a major advancement toward the commercial success of fully integrated silicon photonics.

OCIS codes: (140.5960) Semiconductor lasers; (140.3948) Microcavity devices; (230.5590) Quantum-well, -wire and -dot devices.

http://dx.doi.org/10.1364/OL.41.001664

Optical interconnects have been playing an increasingly important role in high-performance silicon electronics, while high-dissipation electrical-interconnects pose a major roadblock to efficient operation and higher bandwidths [1–4]. To best leverage the economies of scale of silicon, development of complementary metal-oxide-semiconductor (CMOS)-compatible optical components is of paramount importance [5–7]. Monolithic growth of III–V photonic materials on silicon provides the best route toward low-cost and scalable integration, provided crystal defects associated with material incompatibility can be sufficiently reduced [8]. Of the suite of optical components, highly efficient long-wavelength lasers are the most sensitive monitors of the quality of III–V/silicon hetero-integration [1]. Quantum dot (QD) active layers grown on lattice-matched substrates have already shown their capability for lasers with low-threshold densities and temperature-independent operation [9,10]. In addition, the reduced sensitivity of QDs to defects and their unique capability of filtering dislocations make them an ideal candidate for the active layers of hetero-integrated III–V on Si optical sources [11,12]. In this Letter, we utilized InAs QDs monolithically grown on pre-patterned on-axis (001) Si substrates to achieve room-temperature continuous-wave (CW) lasing in a micro-disk resonator. The micro-disk cavities allow for rapid feedback of the QD performance and promote high-quality factor and dense integration for short-reach communication links [13]. The emission is in the 1.3 μm telecommunication band, with low thresholds down to a few hundreds of microwatts. Thus, the InAs QD micro-disk lasers fabricated on Si (001) substrates without intervention of thick and absorptive buffer layers hold high promise for cost-effective integration of low-threshold optical sources on Si.

There has been much recent progress for InAs/GaAs quantum dot (QD) lasers monolithically grown on Ge or Ge-on-Si substrates [14–19], where intermediate buffer layers are used to reduce the number of dislocations and their intrusion into the active layer of the laser. These intermediate buffers, typically germanium and subsequent dislocation filter layers, are absorptive and relatively thick. Such layers limit efficient coupling from the active laser regions to silicon waveguides and preclude potential incorporation in the extensive SOI technology well developed in silicon photonics [8]. Furthermore, the requirement of using few-degree offcut Si substrates for antiphase domain (APD) suppression inevitably compromises its full

compatibility with the prevailing Si CMOS manufacturing processes.

To bypass the need for the absorptive buffer layers and offcut Si substrates, we have recently demonstrated highly ordered, regular arrays of planar GaAs nanowires on industrial-standard (001) silicon by combining the epitaxial necking effect with a design of diamond-shaped Si pockets [20]. Coalescence of these planar nanowires led to high-quality, antiphase-domain-free GaAs-on-V-grooved-Si (GoVS) templates. On the GoVS templates, InAs QDs showed superior structural and optical properties over those grown on conventional offcut Si substrates [21]. Therefore, the GoVS template forms the initial platform of our devices. We grew the GoVS template with 1 μm GaAs coalesced thin film in an Aixtron AIX-200/4 metal-organic chemical vapor deposition (MOCVD) system, using the same procedure [Fig. 1(a)], as detailed in [20]. A root-mean-square roughness of ∼2 nm across a scanning area of 5 μm × 5 μm on the as-grown GoVS template was obtained by atomic force microscopy (AFM) measurements [Fig. 1(b)]. The coalesced thin films are so flat that additional chemical mechanical polishing (CMP) is not needed before QD growth. The defect density in the GaAs layer of the GoVS template is estimated to be on the order of $\sim 10^8$ cm^{-2} by plan-view transmission electron microscopy (TEM). Both TEM and x-ray diffraction suggest a three- to four-fold reduction of defects, as compared to blanket heteroepitaxy of GaAs on offcut Si wafers [21]. Figure 1(c) shows a schematic illustration of the epitaxial layers. The micro-disk laser structure, which is composed of a 1 μm GaAs buffer, a 600 nm $Al_{0.7}Ga_{0.3}As$ post region, and a 500 nm disk region, was grown in a molecular beam epitaxy (MBE) system [22]. We have deployed a five-layer InAs/InGaAs dot-in-a-well (DWELL) structure in the disk region, where the five stacked InAs quantum dots embedded in $In_{0.15}Ga_{0.85}As$ quantum wells are separated by 37.5 nm GaAs barriers and enclosed by outer 50 nm thick $Al_{0.4}Ga_{0.6}As$ barriers. The density of the quantum dots is roughly 4.3×10^{10} cm^{-2}. Figures 1(d) and 1(e) display high-resolution TEM images of the hetero-interface between GaAs and Si. The 4.1% lattice mismatch is accommodated by the formation of a few nanometer-thick stacking faults, mostly trapped within the diamond-shaped pockets [Fig. 1(f)]. In Fig. 1(g), we compare room temperature photoluminescence (PL) from the as-grown laser structure on the GoVS template and a GaAs substrate at a pump power density of 4.7 kW/cm^2. The peak PL intensity from the QDs on GoVS is about 2.5 times lower than the QDs grown on GaAs, with an 18 nm blueshift in the peak wavelength. The high pump power results in the saturation of ground state emission which centers in the 1.3 μm telecommunication band and gives rise to emissions from excited states on the high energy side.

The micro-disks were fabricated using 4 μm silica beads dispersed onto the samples as hard masks for a subsequent ion-assisted etching process. After delineation of the cylinder mesa feature, acetone in an ultrasonic bath was used to remove the remaining SiO_2 microspheres. The pedestal layer was defined by subsequent immersion in a 5% HF solution, which has extreme selectivity in etching AlGaAs with high Al composition in preference to the GaAs disk area. The disk was undercut by ∼1.6 μm laterally from the outer periphery to achieve effective confinement of the optical modes and avoid leakage into the substrate through evanescent wave coupling. Figures 2(a) and 2(b) present 90° and 70° tilted scanning electron microscope (SEM) images of one micro-disk on silicon, revealing a straight vertical etching profile and smooth sidewall surface, crucial for the quality of the resonant modes. Figure 2(c) presents a top-down view of the micro-disk, showing its circular geometry.

The fabricated devices were characterized in a micro-photoluminescence (μPL) system at room temperature. The sample was excited by a 532 nm CW diode laser with spot size focused to approximately 4 μm in diameter. Figure 3(a) shows a representative set of spectra measured from a 4 μm diameter micro-disk on silicon with progressively higher pump power from a 532 nm CW diode laser, denoting the transition from the spontaneous emission regime to the laser oscillation regime. At a low pump intensity of 165 μW, we observe a weak cavity mode at 1308 nm accompanied by a broad background emission. The sub-threshold emission was fit with bi-Lorentzian curves to extract the broad InAs QDs PL background and the narrow cavity emission, as shown in Fig. 3(b). The extracted

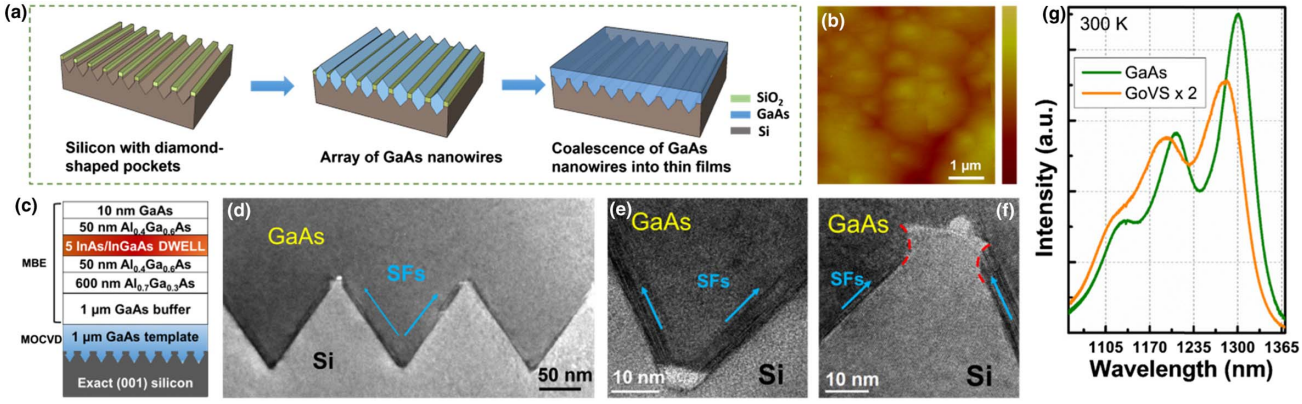

Fig. 1. Epitaxial InAs QDs micro-disks on GoVS substrate. (a) Procedure of growing antiphase-domain-free GaAs thin films out of a highly ordered array of planar GaAs nanowires on silicon substrates with diamond-shaped pockets. (b) AFM image of approximately 1 μm coalesced GaAs thin film grown on the nanowire arrays. The vertical bar is 25 nm. (c) Schematic of the as-grown structure of micro-disk lasers. (d)–(f) Cross-sectional TEM images of the V-grooved structure, showing stacking faults (indicated by the blue arrows) trapped by the Si pockets. (g) Room temperature photoluminescence spectra of the as grown structures on the GoVS template and a GaAs substrate at a pump power density of 4.7 kW/cm^2.

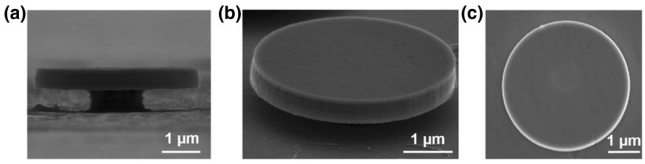

Fig. 2. SEM images of a 4 μm fabricated micro-disk. (a) 90° tilted view of the disk, showing vertical profile. (b) 70° tilted view of the disk, revealing smooth sidewall. (c) Top-down view of the disk, showing circularity.

cavity emission exhibits a small full width at half-maximum (FWHM) of 0.27 nm [Fig. 3(c)]. The cold cavity quality factor Q was calculated accordingly to be $\lambda/\Delta\lambda = 4844$. This is close to the resolution limit of our spectrometer. The peak increases sharply in intensity with further increase of the pump power. The above-threshold spectrum in Fig. 3(d) exhibits a pronounced peak superimposed on a weak background emission with a high aspect ratio of ~10 dB. In Fig. 3(e), the lasing power as a function of pump power (L–L curve) is plotted in the log-log scale, exhibiting clear S-shaped nonlinear characteristics, a clear sign of lasing. The threshold is extrapolated to be ~200 μW.

We simultaneously fabricated micro-disk cavities on the GoVS template and on a GaAs substrate with an identical cavity design for benchmarking. Statistical analysis over a significant sampling of micro-disks was performed to reach a fair comparison by taking into account process variations. Figures 4(a) and 4(b) present the histograms of the lasing wavelength for each measured micro-disk on the GoVS template and GaAs substrate, respectively. The histograms are overlaid with the normalized photoluminescence spectrum of the unprocessed sample. The number on top of each histogram bar denotes the average lasing threshold of the devices. The threshold power and central wavelength of the dominant mode are shown in Fig. 4(c) for concurrent evaluation.

The most dominant lasing modes spotlight optical transitions that are best coupled to the cavity, owing to advantages in radiative emission rate, spatial overlap with a cavity mode, or resonance in frequency [23]. The spread of the central wavelengths in the measured samples is foreseeable, if one considers the distribution of QD density and their varied overlap with the modes of the micro-disks. The threshold is lowest around 1.3 μm, where lasing takes place at a wavelength close to the center of the broad gain spectrum, providing the strongest spatial overlapping of emitters to the surrounding cavity. Lasing modes are mostly observed on the low-energy side of the spectrum, as high-energy photons are more likely to be reabsorbed before coupling to cavity modes [24]. The threshold for the micro-disk lasers on the GoVS template ranges from 130 μW to 410 μW, with an average value of 250 μW, approximately 1.4 times the average value for lasers on the GaAs substrate (180 μW). The average threshold of the micro-disk on GoVS corresponds to 50 μW per QD layer, comparable to the best reported values for InAs QD micro-disk lasers with the same cavity size on GaAs in the literature [25]. Better intrinsic performance of the heteroepitaxially grown lasers could be envisaged by reducing nonradiative losses via engineering the design of the initial templates and enhancing the quality of the coalesced GaAs films, as well as improving the uniformity of the quantum dots [26]. In general, a deeper Si recess with a larger aspect ratio is desirable for better defect confinement. Engineering nanowire pitch size is another approach for enhancing material quality. Additionally, the dislocation density in the coalesced GaAs can be reduced through thermal cycle annealing and/or insertion of strained superlattices.

High crystalline quality of the heteroepitaxially grown III–V thin films is proven through the room temperature continuous-wave operation of the optically pumped lasers, which require the most stringent material quality (e.g., compared to electronic devices). The large-area GaAs thin films grown out of dense planar nanowires on silicon provide a straightforward extension of the micro-disk structure toward practical electrically injected

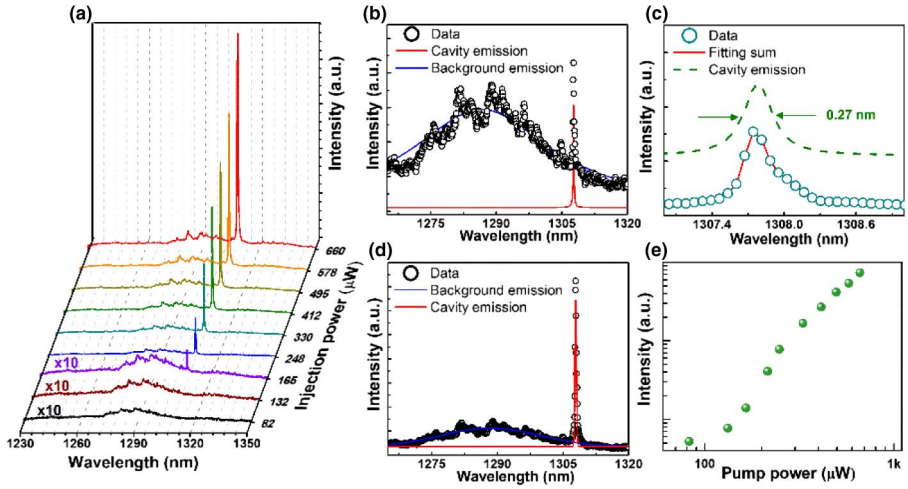

Fig. 3. Laser operation of a 4 μm diameter micro-disk on GoVS. (a) PL spectra taken at increasing pump powers. (b) Sub-threshold spectrum (165 μW). The symbols represent measured data; the blue line is a fit to the broad InAs QDs photoluminescence spectrum background; and the red line is a fit to the narrow cavity emission. (c) High-resolution spectrum at 165 μW. The symbols represent measured data; the red line is a fitting sum of the measured data using bi-Lorentzian curves; and the green line is a fit to the narrow cavity emission. (d) Above-threshold spectrum (248 μW). The symbols represent measured data; the blue line is a fit to the broad InAs QDs photoluminescence spectrum background; and the red line is a fit to the narrow cavity emission. (e) Integrated photoluminescence intensity of the dominant mode as a function of pump power in the log-log scale.

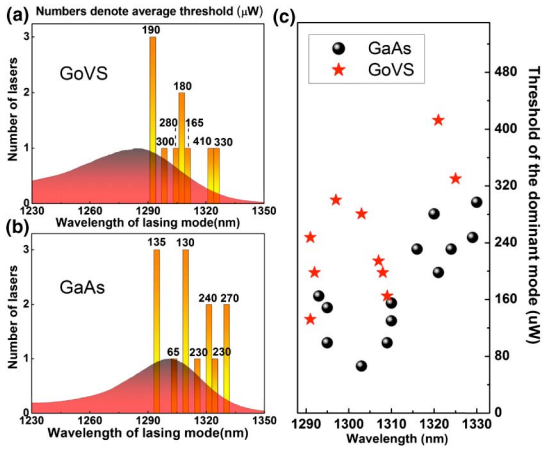

Fig. 4. Statistical analysis of lasing behavior of micro-disks fabricated on GoVS and GaAs. (a), (b) Histogram of the lasing wavelength for each measured device on GoVS and GaAs, respectively. The average lasing threshold of the devices within each histogram bar is denoted by the number displayed on top of it. The normalized photoluminescence spectrum of the unprocessed sample is denoted in red. (c) Lasing threshold is plotted as a function of a lasing wavelength for micro-disks fabricated on GoVS (red stars) and GaAs (black spheres).

laser configurations [27]. The GaAs planar nanowires are formed using the aspect ratio trapping approach which is well-recognized as a viable integration path for III–V high mobility channel FinFETs on silicon [28,29]. The GoVS templates can thus be envisaged as an extension of III–V fin arrays for optoelectronic devices requiring large active regions, suggesting the possibility of co-integration of silicon photonic and electronic circuits onto the same chip. More importantly, the highly scalable growth technique presented here is extendable to the InP material system, and can be potentially used for the growth of various heterostructures with ternary and quaternary materials, quantum wells, or quantum dots on silicon, as evidenced by a recent report of InP distributed feedback laser arrays directly grown on silicon [30].

In conclusion, we demonstrated the first operation of InAs QD micro-disk lasers on exactly (001)-orientated Si substrates through germanium-free heteroepitaxy. Room-temperature continuous-wave lasing at 1.3 μm has been achieved with very low threshold (200 μW) for a five-layer QD device. This monolithic solution to the long-awaited missing piece of Si photonics marks a major step toward optoelectronics integration on Si for high-performance optical communication and computing applications.

Funding. Research Grants Council, University Grants Committee, Hong Kong (614813, 16212115); Defense Sciences Office, DARPA (MTO EPHI).

Acknowledgment. The authors would like to thank SUNY Poly for providing the initial nano-patterned Si substrates, Wuhan National Laboratory for Optoelectronics (WNLO) for providing facilities to perform optical measurements, and NFF and MCPF of HKUST for technical support. Helpful discussions with C. Zeng, Y. Geng, and B. Shi are also acknowledged.

[†]These authors contributed equally to this work

REFERENCES

1. D. Liang and J. E. Bowers, Nat. Photonics **4**, 511 (2010).
2. Z. Zhou, B. Yin, and J. Michel, Light: Sci. Appl. **4**, e358 (2015).
3. R. Won, Nat. Photonics **4**, 498 (2010).
4. A. E. Lim, J. Song, Q. Fang, C. Li, X. Tu, N. Duan, K. K. Chen, R. P. Tern, and T. Y. Liow, IEEE J. Sel. Top. Quantum Electron. **20**, 405 (2014).
5. G. T. Reed, G. Mashanovich, F. Y. Gardes, and D. J. Thomson, Nat. Photonics **4**, 518 (2010).
6. J. Michel, J. Liu, and L. C. Kimerling, Nat. Photonics **4**, 527 (2010).
7. F. Xia, L. Sekaric, and Y. Vlasov, Nat. Photonics **1**, 65 (2007).
8. J. E. Bowers, J. T. Bovington, A. Y. Liu, and A. C. Gossard, *Optical Fiber Communication Conference* (Optical Society of America, 2014).
9. A. E. Zhukov, M. V. Maksimov, and A. R. Kovsh, Semiconductors **46**, 1249 (2012).
10. M. Sugawara and M. Usami, Nat. Photonics **3**, 30 (2009).
11. J. Yang, P. Bhattacharya, and Z. Mi, IEEE Trans. Electron. Devices **54**, 2849 (2007).
12. D. Bordel, D. Guimard, M. Rajesh, M. Nishioka, E. Augendre, L. Clavelier, and Y. Arakawa, Appl. Phys. Lett. **96**, 043101 (2010).
13. K. J. Vahala, Nature **424**, 839 (2003).
14. H. Liu, T. Wang, Q. Jiang, R. Hogg, F. Tutu, F. Pozzi, and A. Seeds, Nat. Photonics **5**, 416 (2011).
15. A. Lee, Q. Jiang, M. Tang, A. Seeds, and H. Liu, Opt. Express **20**, 22181 (2012).
16. S. M. Chen, M. C. Tang, J. Wu, Q. Jiang, V. G. Dorogan, M. Benamara, Y. I. Mazur, G. J. Salamo, A. J. Seeds, and H. Liu, Electron. Lett. **50**, 1467 (2014).
17. A. Y. Liu, C. Zhang, J. Norman, A. Snyder, D. Lubyshev, J. M. Fastenau, A. W. K. Liu, A. C. Gossard, and J. E. Bowers, Appl. Phys. Lett. **104**, 041104 (2014).
18. A. Y. Liu, R. W. Herrick, O. Ueda, P. M. Petroff, A. C. Gossard, and J. E. Bowers, IEEE J. Sel. Top. Quantum Electron. **21**, 690 (2015).
19. A. Y. Liu, S. Srinivasan, J. Norman, A. C. Gossard, and J. E. Bowers, Photon. Res. **3**, B1 (2015).
20. Q. Li, K. W. Ng, and K. M. Lau, Appl. Phys. Lett. **106**, 072105 (2015).
21. Y. Wan, Q. Li, Y. Geng, B. Shi, and K. M. Lau, Appl. Phys. Lett **107**, 081106 (2015).
22. A. Y. Liu, C. Zhang, A. Snyder, D. Lubyshev, J. M. Fastenau, A. W. K. Liu, A. C. Gossard, and J. E. Bowers, J. Vac. Sci. Technol. B **32**, 02C108 (2014).
23. A. Woolf, T. Puchtler, I. Aharonovich, T. Zhu, N. Niu, D. Wang, R. Oliver, and E. L. Hu, Proc. Natl. Acad. Sci. USA **111**, 14042 (2014).
24. A. C. Tamboli, E. D. Haberer, R. Sharma, K. H. Lee, S. Nakamura, and E. L. Hu, Nat. Photonics **1**, 61 (2007).
25. N. V. Kryzhanovskaya, A. E. Zhukov, M. V. Maximov, E. I. Moiseev, I. I. Shostak, A. M. Nadtochiy, Y. V. Kudashova, A. A. Lipovskii, M. M. Kulagina, and S. I. Troshkov, IEEE J. Sel. Top. Quantum Electron. **21**, 709 (2015).
26. W. W. Chow, A. Y. Liu, A. C. Gossard, and J. E. Bowers, Appl. Phys. Lett. **107**, 171106 (2015).
27. D. Liang, M. Fiorentino, T. Okumura, H. Chang, D. T. Spencer, Y. Kuo, A. W. Fang, D. Dai, R. G. Beausoleil, and J. E. Bowers, Opt. Express, **17**, 20355 (2009).
28. J. A. del Alamo, Nature **479**, 317 (2011).
29. N. Waldron, C. Merckling, W. Guo, P. Ong, L. Teugels, S. Ansar, D. Tsvetanova, F. Sebaai, D. H. van Dorp, A. Milenin, D. Lin, L. Nyns, J. Mitard, A. Pourghaderi, B. Dohaurd, O. Richard, H. Bender, G. Boccardi, M. Caymax, M. Heyns, W. Vandervorst, K. Barla, N. Collaert, and A. V.-Y. Thean, *IEEE Symposium on VLSI Technology: Digest of Technical Papers* (2014), pp. 1–2.
30. Z. Wang, B. Tian, M. Pantouvaki, W. Guo, P. Absil, J. V. Campenhout, C. Merckling, and D. V. Thourhout, Nat. Photonics **9**, 837 (2015).